LASER & PHOTONICS REVIEWS

www.lpr-journal.org

Optically-Controlled Quantum Size Effect in a Hybrid Nanocavity Composed of a Perovskite Nanoparticle and a Thin Gold Film

*Shulei Li, Maohui Yuan, Weijie Zhuang, Xin Zhao, Shaolong Tie, Jin Xiang, and Sheng Lan**

Metal halide perovskites have attracted great interest in recent years and their emission wavelength can be adjusted either by doping impurities or by exploiting quantum size effect. Here, it is reported that the realization of optically-controlled quantum size effect in a hybrid nanocavity composed of a perovskite ($CsPbBr_3$) nanoparticle and a thin gold (Au) film. Such nanocavities are created by synthesizing polycrystalline $CsPbBr_3$ nanoparticles composed of quantum dots on a thin Au film via chemical vapor deposition, which emit luminescence at ≈488 nm under the excitation of femtosecond laser pulses with a low repetition rate. The phase transition from polycrystalline to monocrystalline, which quenches the quantum size effect and shifts the emission wavelength to ≈515 nm, can be introduced in $CsPbBr_3$ nanoparticles by simply increasing the laser power. Interestingly, such a phase transition is reversible provided that the laser power is lower than a threshold. Consequently, four optical states including dual-wavelength emission, can be achieved by deliberately setting the laser power. The underlying physical mechanism is unveiled by the static and transient temperature distributions simulated for the hybrid nanocavity. The findings open a new avenue for designing novel photonic devices based on perovskite nanoparticles and plasmonic nanostructures.

1. Introduction

Metal halide perovskites have attracted great interest in recent years owing to their potential applications in optoelectronic devices such as light-emitting devices,[1–4] photodetectors,[5–7] solar cells,[8–11] and even lasers.[12–14] In particular, much effort has been devoted to $CsPbBr_3$ which generally emits green light. So far, $CsPbBr_3$ films and particles with different feature sizes have been successfully synthesized and most studies focus on quantum dots showing quantum size effect and microparticles supporting whisper galley modes.[15–17] In comparison, less attention has been paid to $CsPbBr_3$ nanoparticles with diameters ranging from 50 to 500 nm, which exhibit Mie resonances in the visible to near-infrared spectral range. As compared with high-index semiconductors such as Si, Ge, and GaAs, $CsPbBr_3$ possesses a moderate refractive index (≈2.0) which is large enough to support distinct Mie resonances.[18–21] Actually, the Fano resonances formed by the interaction between the Mie resonances and the excitonic ones in $CsPbBr_3$ nanoparticles have been observed.[20] In addition, the optical resonances supported by $CsPbBr_3$ nanoparticles have been exploited to enhance their nonlinear optical responses and to realize strong light–matter interaction and even lasing.[19]

It has been known that strongly-localized electric field can be achieved at the gap region between a dielectric nanoparticle and a thin metal film, which has been employed to construct nanoscale photonic devices with different functionalities.[22–26] Therefore, it is expected that the interaction of a $CsPbBr_3$ nanoparticle with light can be enhanced by placing the nanoparticle on a thin metal film, forming a particle-on-film system or a hybrid nanocavity. The nanocavities created in this way generally possess gap modes and mirror image modes induced by the metal film, where the strong localization of electric field can be achieved. As a result, both the absorption and emission efficiencies of the nanoparticle will be greatly enhanced. Previously, the hybrid nanocavities formed by silicon (Si) nanoparticles and a thin metal film have been employed to realize nanoscale

S. Li, Dr. M. Yuan, W. Zhuang, X. Zhao, Prof. S. Lan
Guangdong Provincial Key Laboratory of Nanophotonic Functional Materials and Devices School of Information and Optoelectronic Science and Engineering
South China Normal University
Guangzhou 510006, P. R. China
E-mail: slan@scnu.edu.cn

Prof. S. Tie
School of Chemistry
South China Normal University
Guangzhou 510006, P. R. China

Dr. J. Xiang
Department of Electrical and Computer Engineering
University of Wisconsin–Madison
Madison WI 53705, USA

The ORCID identification number(s) for the author(s) of this article can be found under https://doi.org/10.1002/lpor.202000480

DOI: 10.1002/lpor.202000480

photonic devices for practical applications of optical display, sensing, luminescence enhancement, and strong light–matter interaction.[27,28] Apart from the localization of electric field and the modification of absorption/emission properties, the thin metal film with good thermal conductivity also acts as a heat sink for nanoparticles, preventing them from being damaged and modifying the temperature distributions in the nanoparticles.

So far, perovskite nanoparticles (including $CsPbBr_3$) have been successfully fabricated by using different methods, such as hot injection synthesis,[29] spin-coating,[30] ligand-assisted reprecipitation,[31,32] chemical vapor deposition,[33] etc. In most cases, the chemical reactions are precisely controlled in order to obtain monocrystalline materials. For compound semiconductors, however, polycrystalline nanoparticles are usually obtained because of the deviation from chemical ratio. For example, GaAs nanoparticles fabricated by using femtosecond laser ablation under the nonequilibrium condition are generally polycrystalline.[34] In this case, the phase transition from polycrystalline to monocrystalline occurs if a post-annealing process is employed. Previous studies reveal that quantum size effect becomes significant for perovskite nanocrystals smaller than 5 nm.[35–37] For this reason, such nanocrystals are generally referred to as quantum dots. If a polycrystalline nanoparticle is composed of a number of quantum dots, it may exhibit optical properties similar to single quantum dots.[38] A direct consequence is the blueshift of the emission wavelength with respect to that of a monocrystalline nanoparticle. From the viewpoint of fabrication, such a polycrystalline nanoparticle can be obtained by using a low growth temperature.

It is well known that perovskites are generally not stable against light irradiation, leading to ion segregation, decomposition, and phase transition. Very recently, it was demonstrated that photoinduced halide-ion segregation, which is dependent on the carrier-induced strain gradients vanishing at sufficiently high carrier densities, can be actively controlled in situ with light.[39–41] In principle, the phase transition from polycrystalline to monocrystalline in a nanoparticle can be accurately controlled via laser-induced annealing if a spatially-localized temperature distribution can be established inside the nanoparticle. In this case, the nanoparticle is a mixture of polycrystal and monocrystal, leading to a dual-wavelength emission with controllable emission intensities, which is quite useful for optical display, sensing, and signal processing. Previously, spatially-localized temperature distribution was successfully achieved by exploiting the Fano resonance formed in an oligomer of gold (Au) nanoparticles.[42] It was used to produce carbon quantum dots with small diameters, which emit efficient luminescence in the visible light spectrum. As mentioned above, the strongly-localized electric field achieved in the gap region between a dielectric nanoparticle and a thin metal film has been exploited to construct nanoscale photonic devices with different functionalities.[22–25] Therefore, it is expected that the controllable phase transition from polycrystalline to monocrystalline might be possible by exploiting the strongly-localized electric field in a hybrid nanocavity composed of a perovskite nanoparticle and a thin metal film.

In this communication, we proposed a hybrid nanocavity composed of a $CsPbBr_3$ nanoparticle and a thin Au film and demonstrated optically-controlled quantum size effect in such a nanocavity by exploiting the reversible phase transition from polycrystalline to monocrystalline in the $CsPbBr_3$ nanoparticle. This unique feature of the hybrid nanocavity makes it possible to realize nanoscale light source with dual-wavelength emission and four controllable optical states for optical signal processing.

2. Results and Discussion

Spherical $CsPbBr_3$ nanoparticles with diameters (d) ranging from 50 to 500 nm were synthesized on a thin Au film by using chemical vapor deposition at temperature (870 K), as shown in **Figure 1**a where the scanning electron microscopy (SEM) images of such $CsPbBr_3$ nanoparticles are presented. From the magnified image shown in the inset, it was found that the surfaces of such $CsPbBr_3$ nanoparticles are not smooth. In Figure 1b, we show the energy dispersive spectroscopy (EDS) mapping carried out for a typical $CsPbBr_3$ nanoparticle, which indicates the uniform spatial distribution of the constituent elements (i.e., Cs, Pb, and Br). We also examined the crystalline structure of the as-prepared nanoparticles by using transmission electron microscopy (TEM). A typical example is shown in Figure 1c where a small nanoparticle with $d \approx 100$ nm was selected in order to clearly reveal the internal structure. It was found that the as-prepared nanoparticle consists of a large number of quantum dots with sizes smaller than 5.0 nm. Accordingly, Debby–Sherrer rings, which are the characteristics of a polycrystal, were observed in the electron diffraction pattern. Surprisingly, a gradual change in the internal structure of the nanoparticle occurred during the TEM measurements, as shown in Figure 1c. Upon the irradiation of high-energy electron beam, the quantum dots inside the nanoparticle gradually merged into nanocrystals with larger sizes. Meanwhile, the Debby–Sherrer rings in the electron diffraction pattern evolved into discrete diffraction spots. Finally, a monocrystalline $CsPbBr_3$ nanoparticle, which is manifested in the Bragg diffraction spots, was obtained. The electron diffraction pattern after the phase transition matches well with the cubic phase of $CsPbBr_3$. The lattice spacing, which was estimated to be ≈0.29 nm, corresponds to the lattice spacing of Pb atomic layers in $CsPbBr_3$ crystals (Figure S1, Supporting Information).[43] In Figure 1d, we show the Raman spectra measured for a $CsPbBr_3$ nanoparticle, in which the vibrational modes of the $CsPbBr_3$ sublattice are revealed, including a strong (Raman active) mode at 71 cm^{-1} and two weak modes at 125 and 311 cm^{-1}.[44,45] Figure 1e shows the up-converted photoluminescence (PL) spectra measured at different laser powers for a $CsPbBr_3$ nanoparticle, which was excited by using 800-nm femtosecond laser pulses with a high repetition rate of 76 MHz. Surprisingly, the luminescence of the $CsPbBr_3$ nanoparticle exhibited only a single emission peak ≈515 nm, which is different from the emission wavelength of $CsPbBr_3$ quantum dots generally appearing at a shorter wavelength of ≈488 nm due to quantum size effect.[46] Based on the phase transition phenomenon observed in the TEM measurements, we suspected that the phase transition in the $CsPbBr_3$ nanoparticle was completed in a short time upon the irradiation of femtosecond laser pulses with a high repetition rate of 76 MHz. In the inset of Figure 1e, we show the dependence of the luminescence intensity on the laser power (P) plotted in a logarithmic coordinate. The luminescence intensity increased gradually at low laser powers with a slope of ≈0.92, which is smaller than the value expected for up-converted

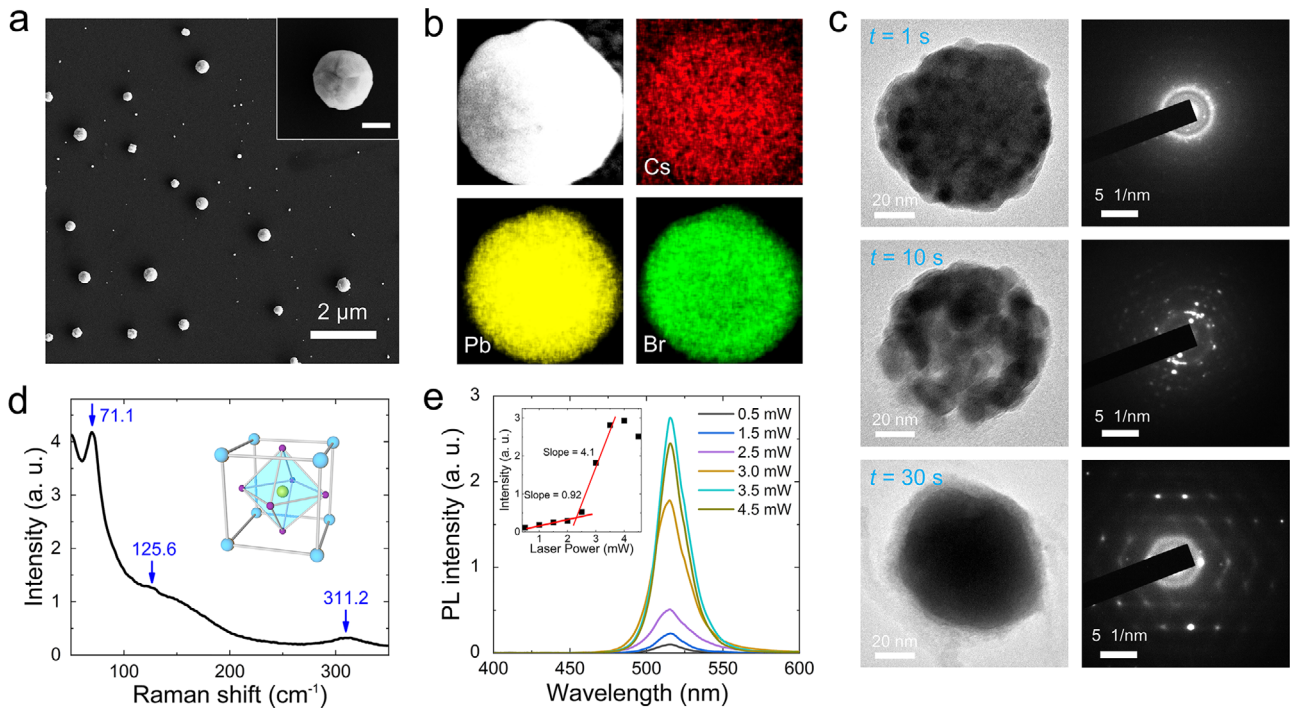

Figure 1. a) SEM image of the $CsPbBr_3$ nanoparticles synthesized on a thin Au film via chemical vapor deposition. The magnified image of a typical $CsPbBr_3$ nanoparticle is shown in the inset (the length of the scale bar is 200 nm). b) EDS mapping of Cs, Pb, Br for a $CsPbBr_3$ nanoparticle. c) Phase transition of a $CsPbBr_3$ nanoparticle from polycrystalline to monocrystalline induced by irradiating high-energy electron beam during the TEM characterization (left panel). Also shown is the change in the electron diffraction pattern (right panel). d) Raman spectrum measured for a $CsPbBr_3$ nanoparticle. The crystal structure of $CsPbBr_3$ is shown in the inset. e) PL spectra measured for a $CsPbBr_3$ nanoparticle excited by using 800-nm femtosecond laser pulses of 76 MHz at different laser powers. The dependence of the PL intensity on the excitation power is shown in the inset.

luminescence (>2.0). This behavior is ascribed to the drastic changes of the attributes of the hybrid nanocavity induced by the phase transition of the $CsPbBr_3$ nanoparticle, including two-photon-induced absorption (TPA) cross-section, field enhancement factor, and emission quantum efficiency. In this case, part of the energy absorbed by the $CsPbBr_3$ nanoparticle might be converted to heat for the growth of nanocrystals. We also examined the dependence of the luminescence intensity on the laser power for $CsPbBr_3$ nanoparticles after the phase transition (Figure S2, Supporting Information). A single slope of ≈2.2 was observed, implying the up-converted luminescence is caused mainly by TPA process. When the laser power exceeds ≈1.7 mW, a rapid increase in the luminescence intensity was observed, giving a slope of ≈4.1. Unfortunately, the saturation of the luminescence intensity occurred for laser powers larger than 2.2 mW, possibly due to the photon-induced decomposition of $CsPbBr_3$, which is commonly observed for $CsPbBr_3$ quantum dots or nanocrystals.[47,48]

Since $CsPbBr_3$ nanoparticles were prepared on a thin Au film, they can create hybrid nanocavities with the Au film. Therefore, we need to find out the optical modes supported by such nanocavities and the electric field enhancements achieved at these optical modes which can be exploited to improve the linear and nonlinear optical responses of $CsPbBr_3$ nanoparticles. **Figure 2**a shows the forward scattering spectra calculated for $CsPbBr_3$ nanoparticles with different diameters (d = 100–400 nm) placed on a 50-nm-thick Au film. The luminescence spectrum of $CsPbBr_3$ is also provided for reference. For d = 100 nm, the scattering peak appears at ≈550 nm. With increasing diameter, a small shoulder emerges at the short wavelength side and it evolves gradually into a second peak at ≈500 nm for d = 280 nm. After that, the intensity of this peak exceeds that of the first one and becomes dominant for d = 340 nm. For d = 400 nm, only a single scattering peak located exactly at the absorption peak (≈515 nm) is observed. This feature remains unchanged for nanoparticles with d > 400 nm and it will be used later to judge the phase transition because the forward scattering spectra of $CsPbBr_3$ nanoparticles on the Au film can be easily measured by using conventional dark-field microscopy. Since $CsPbBr_3$ nanoparticles are excited by using femtosecond laser light from top, we need to examine the backward scattering spectra of $CsPbBr_3$ nanoparticles from which the electric field enhancement can be extracted. In Figure 2b–d, we show the backward scattering spectra calculated for $CsPbBr_3$ nanoparticles with d = 300, 400, and 500 nm, respectively. In each case, the spectrum of $[\int|E(\lambda)|^4 dV]/V$ (V is the volume of the $CsPbBr_3$ nanoparticle, λ is the wavelength of light), which is generally employed to evaluate the TPA of a nanoparticle,[34,49,50] is also presented. It is remarkable that the largest value of $\int|E(\lambda)|^4 dV]/V$ at the excitation wavelength (800 nm) is achieved in the $CsPbBr_3$ nanoparticle with d ≈ 400 nm, implying an enhanced TPA. Similar to $[\int|E(\lambda)|^4 dV]/V$, the spectrum of $[\int|E(\lambda)|^2 dV]/V$ can be used to characterize the emission efficiencies at different wavelengths because the quantum transition rate is proportional to the local density of state.[23,50] From the

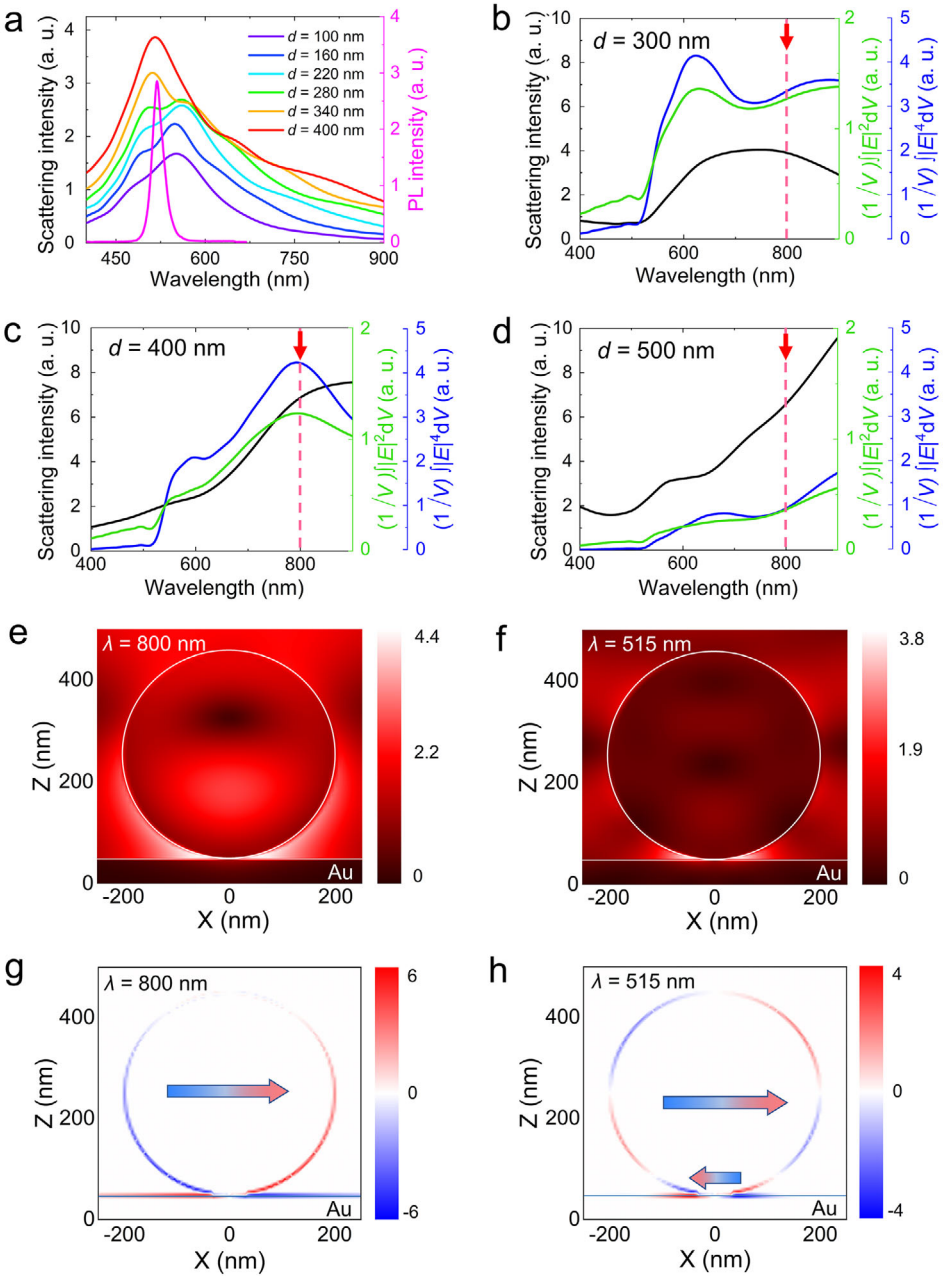

Figure 2. a) Forward scattering spectra calculated for $CsPbBr_3$ nanoparticles with different diameters placed on an Au film. b–d) Backward scattering spectra, $[\int|E(\lambda)|^2 dV]/V$ and $[\int|E(\lambda)|^4 dV]/V$ spectra calculated for $CsPbBr_3$ nanoparticles with diameters of 300, 400, and 500 nm. e,f) Electric field distributions calculated for a $CsPbBr_3$ nanoparticle with $d = 400$ nm at 515 and 800 nm. The corresponding electric charge distributions are shown in (g) and (h), respectively.

spectra of $[\int|E(\lambda)|^2 dV]/V$ shown in Figure 2b–d, it is found that the emission efficiency at the emission wavelength of $CsPbBr_3$ (≈515 nm) decreases with increasing diameter and a moderate value is obtained for the $CsPbBr_3$ nanoparticle with $d \approx 400$ nm. As compared with the $CsPbBr_3$ nanoparticles placed on a silica (SiO_2) substrate, the absorption and emission efficiencies are greatly enhanced owing to the introduction of the thin Au film (Figure S3, Supporting Information). Actually, the enhancements in the absorption and emission efficiencies can be visualized in the electric field distributions calculated for the nanoparticle with $d = 400$ nm at $\lambda = 800$ and 515 nm, as shown in Figure 2e,f (Figure S4, Supporting Information). In both cases, it can be seen that an enhancement in the electric field is observed in the gap region between the nanoparticle and the Au film. In order to identify the physical origins of the optical modes, we calculated the electric charge distributions at $\lambda = 800$ and 515 nm, as shown in Figure 2g,h. From the electric charge distribution at $\lambda = 800$ nm, one can identify an electric dipole mode and a gap

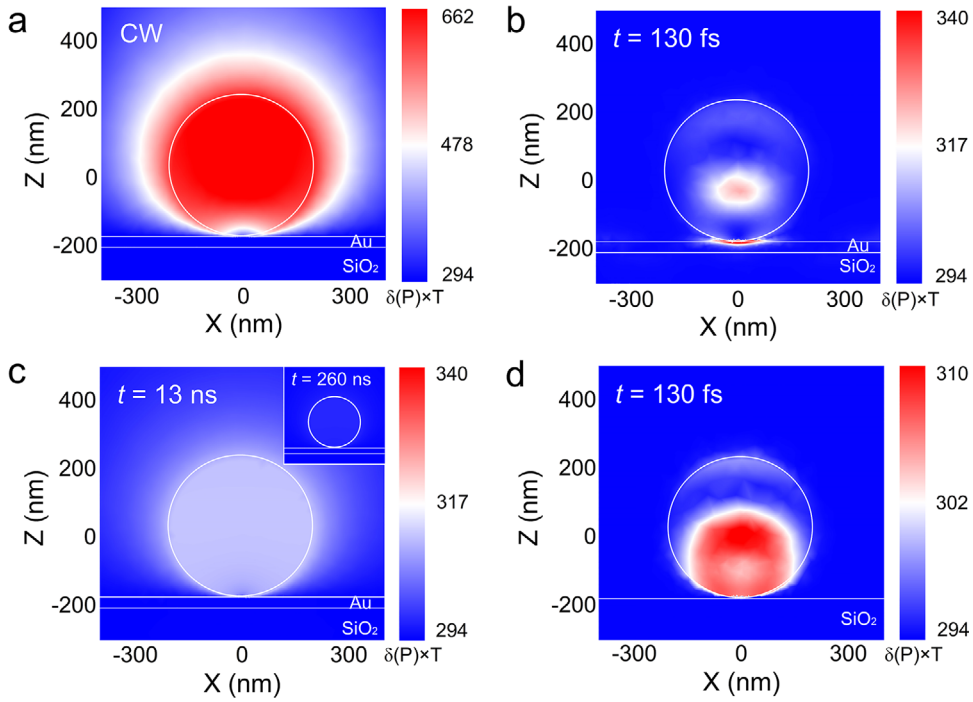

Figure 3. a) Static temperature distribution in the XZ plane calculated for a $CsPbBr_3$ nanoparticle placed on an Au film and excited by using a continuous wave laser light at 800 nm. b) Transient temperature distribution in the XZ plane (t = 130 fs) calculated for a $CsPbBr_3$ nanoparticle on an Au film after being excited by using a single 800-nm femtosecond laser pulse with a duration of 130 fs. c) Transient temperature distribution in the XZ plane (t = 13 ns) calculated for a $CsPbBr_3$ nanoparticle on an Au film after being excited by using a single 800-nm femtosecond laser pulse with a duration of 130 fs. The transient temperature distribution at t = 260 ns is shown in the inset. d) Transient temperature distribution in the XZ plane (t = 130 fs) calculated for a $CsPbBr_3$ nanoparticle placed on a SiO_2 substrate after being excited by using a single 800-nm femtosecond laser pulse with a duration of 130 fs.

mode. In comparison, an electric quadrupole mode is revealed from the electric charge distribution at λ = 515 nm.

As demonstrated above, strongly-localized electric field can be achieved at the gap region between the nanoparticle and the Au film (see Figure 2e). It is interesting to know whether the strongly-localized electric field can lead to a spatially-localized temperature distribution. So far, it remains a significant challenge to measure the temperature of a nanoparticle, even in the steady-state. In this work, we employed numerical simulation to investigate the temperature change induced in the nanoparticle by femtosecond laser pulses. In order to examine the influence of the thin Au film on the temperature distribution inside the nanoparticle, we have calculated the temperature distributions in the hybrid nanocavity under different excitation conditions, as shown in **Figure 3**a–c. In Figure 3a, we show the static temperature distribution achieved in the hybrid nanocavity under the excitation of continuous-wave laser light. In this case, the highest temperature is achieved at the center of the $CsPbBr_3$ nanoparticle due to heat accumulation effect. Owing to the good conductivity of the Au film, the lowest temperature inside the nanoparticle is observed at the contact point between the nanoparticle and the Au film. It is noticed that the temperature distribution is almost uniform inside the nanoparticle, implying that the phase transition from polycrystalline to monocrystalline will occur over the whole nanoparticle once the temperature exceeds a critical value. Therefore, it is difficult to observe the polycrystalline phase or the coexistence of the two phases when continuous wave laser light is employed to excite the nanoparticle. The temperature distribution in the hybrid nanocavity induced by using a single femtosecond laser pulse of 130 fs is shown in Figure 3b. It is remarkable that a spatially-localized temperature distribution is achieved at the contact point between the nanoparticle and the Au film, quite similar to the electric field distribution shown in Figure 2e. The temperature distributions after 13 and 260 ns of the first pulse (or before the arrival of the second pulse), which correspond to femtosecond laser pulses with repetition rates of 76 and 3.8 MHz, are presented in Figure 3c. It is noticed that the temperature inside the nanoparticle is still higher than the environment temperature after 13 ns, implying the existence of heat accumulation. In sharp contrast, the nanoparticle is cooled down to room temperature after 260 ns. This behavior indicates that the static temperature distribution in the hybrid nanocavity under the excitation of femtosecond laser pulses of 76 MHz will eventually approach that obtained by using continuous-wave laser light. Differently, the temperature distribution in the hybrid nanocavity induced by using femtosecond laser pulses of 3.8 MHz will exhibit the same one as that obtained by using a single femtosecond laser pulse. Apparently, the spatially-localized temperature distribution achieved in this case enables the control of the phase transition volume inside the nanoparticle and thus the relative intensities of the two emission wavelengths. For comparison, we also calculated the temperature distribution of a $CsPbBr_3$ nanoparticle (d = 400 nm) placed on a SiO_2 substrate, which is excited by using a single femtosecond laser pulse of

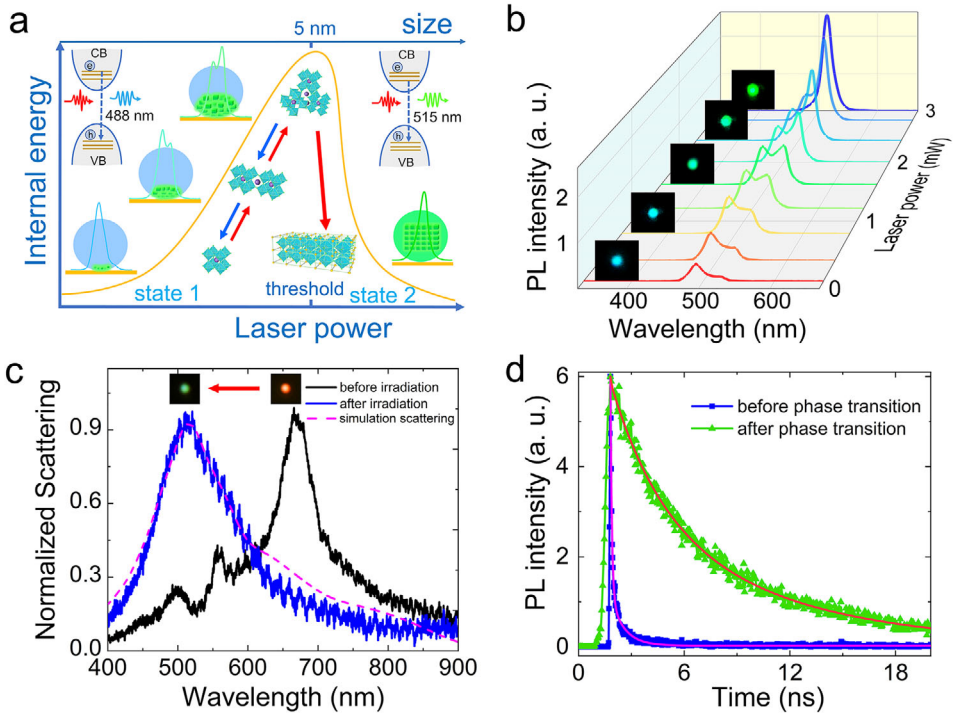

Figure 4. a) Schematic showing the controllable phase transition from polycrystalline to monocrystalline manipulated by adjusting the laser power. b) Evolution of the PL spectrum of a $CsPbBr_3$ nanoparticle with increasing laser power. The CCD images of the PL at different laser powers are shown in the insets. c) Forward scattering spectra measured for a $CsPbBr_3$ nanoparticle before and after the phase transition. In both cases, the scattering intensities have been normalized. The scattering spectrum simulated for a monocrystalline $CsPbBr_3$ nanoparticle with $d = 400$ nm (dashed curve) is also provided for comparison. The CCD images of the scattering light are shown in the insets. d) PL decays measured for a $CsPbBr_3$ nanoparticle before and after the phase transition. In both cases, the PL decays are fitted by biexponential decay functions with two-time constants.

130 fs (see Figure 3d). It can be seen that the localization of temperature and controllable phase transition are not available in this case due to the small thermal conductivity of SiO_2.

Based on the temperature distribution simulated for the hybrid cavity, it is predicted that spatially-localized temperature distribution can be achieved at the contacting point between the $CsPbBr_3$ nanoparticle and the Au film when femtosecond laser pulses with a low repetition rate are employed as the excitation source. This intriguing feature makes it possible to control the volume of phase transition inside the nanoparticle, realizing optically-controlled quantum size effect and dual-wavelength emission.[51] In **Figure 4**a, we present a schematic illustrating the phase transition occurring in the $CsPbBr_3$ nanoparticle. Upon the irradiation of femtosecond laser light, the annealing process leading to the merge of small quantum dots into a larger nanocrystal starts from the bottom of the nanoparticle. However, the nanocrystal obtained in this way is not stable if its volume is not large enough. As a result, it will be decomposed into small quantum dots again if the local temperature is reduced, leading to a reversible phase transition. Once the volume of the nanocrystal approaches that of the nanoparticle, the whole nanoparticle could be transformed into monocrystalline state with a lower energy. In this case, an excess energy is necessary for decomposing the nanocrystal into small quantum dots and the reverse phase transition is inhibited. Based on the analysis of the optical modes supported by the nanocavity, we chose to excite a $CsPbBr_3$ nanoparticle with $d \approx 400$ nm by using 800-nm femtosecond laser pulses with a low repetition rate of 3.8 MHz. The evolution of the luminescence spectrum with increasing laser power is presented in Figure 4b. Different from the typical luminescence spectrum of a $CsPbBr_3$ nanoparticle which exhibits a single peak at ≈515 nm (see Figure 1e), two distinct peaks centered at ≈495 and ≈520 nm are observed. As expected, the relative intensities of the two peaks can be manipulated by simply varying the excitation laser power. It means that single-wavelength emission at either 495 or 520 nm and dual-wavelength emission with equal intensities can be realized by deliberately controlling the excitation laser power (Figure S5, Supporting Information). This process is repeatable provided that the laser power is lower than a threshold, which is estimated to be ≈2.0 mW. If the laser power exceeds the threshold, the emission wavelength is blue-shifted to ≈515 nm and it remains unchanged with increasing laser power, corresponding to the phase transition from polycrystalline to monocrystalline (Figure S6, Supporting Information). In this work, we examined the threshold for the phase transition by using femtosecond laser pulses with two repetition rates of 3.8 and 2.9 MHz. It was found that the threshold for the phase transition increases with decreasing repetition rate. The threshold is increased from 2.0 to 2.5 mW when the repletion rate is reduced from 3.8 to 2.9 MHz. We did not carry experiments by using femtosecond laser pulses with repetition rates lower than 2.9 MHz because the maximum laser power available was not enough to induce the phase transition. In order to confirm the phase transition, we examined the forward scattering spectra of

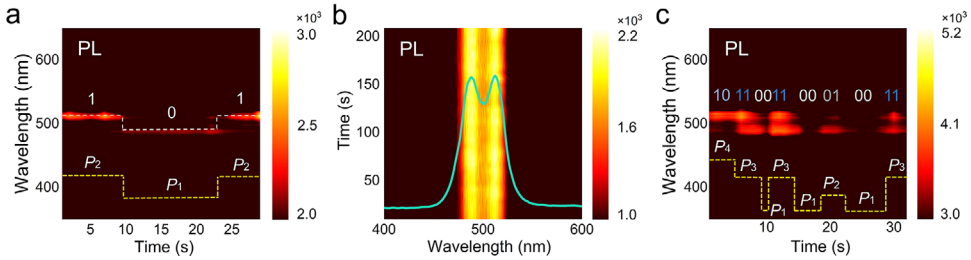

Figure 5. a) Controlling the emission wavelength of a hybrid nanocavity by adjusting the laser power. b) Stable dual-wavelength emission from the hybrid nanocavity. c) Four optical states (i.e., 00, 01, 10, and 11) generated by controlling the laser power.

the nanoparticle before and after the phase transition, as shown in Figure 4c. The scattering peak of the nanoparticle initially appears at ≈670 nm. It is blue-shifted to ≈515 nm after the phase transition. Accordingly, the scattering light is changed from red to green, as shown in the inset. It is noticed that the measured scattering spectrum after the phase transition agrees well with the simulated one (dashed curve, see also Figure 2a). It implies that the nanoparticle is really composed of monocrystalline $CsPbBr_3$ whose refractive index is adopted to calculate the scattering spectrum. We also compared the luminescence lifetimes of the nanoparticle before and after the phase transition, as shown in Figure 4d. In both cases, the luminescence decays can be fitted by bi-exponential decays with two-time constants (τ_1 and τ_2). It was found that the dominant lifetime (τ_1), which is initially ≈79 ps, is greatly prolonged to ≈2.8 ns after the phase transition. The luminescence lifetimes before and after the phase transition are in good agreement with those reported previously for $CsPbBr_3$ quantum dots and large nanocrystals.[51,52]

The hybrid nanocavities proposed and investigated in this work may have many potential applications due to their unique dual-wavelength emission which can be manipulated by simply adjusting the excitation laser power. This intriguing property originates from the controllable and reversible phase transition from polycrystalline to monocrystalline induced by laser heating. As an example, we demonstrated the realization of single- and dual-wavelength emissions with equal intensities by controlling the excitation laser power, as shown in **Figure 5**a,b. In this experiment, we used 800-nm femtosecond laser pulses with a repetition of 3.8 MHz and average powers smaller than 2.0 mW (i.e., the threshold) to excite the hybrid nanocavity. As shown in Figure 5a, the emission at 495 nm is much stronger than that at 520 nm when the laser power is chosen to be $P_1 = 1.2$ mW. However, the situation is reversed when the laser power is raised to $P_2 = 1.6$ mW. In both cases, the hybrid nanocavity can be considered as a single-wavelength light source. An intermediate state where the intensities at the two emission wavelengths are equal is achieved when the laser power is set to be $P = 1.4$ mW, as shown in Figure 5b. In this case, the hybrid nanocavity serves as a dual-wavelength light source. The scattering spectrum of the hybrid nanocavity was monitored during the operation. No obvious change is observed in the scattering spectrum, implying that the $CsPbBr_3$ nanoparticle is stable under the excitation of low-power laser light (Figure S7, Supporting Information). The controllable dual-wavelength emission from the hybrid nanocavity offers us the opportunity of generating four optical states (i.e., 00, 10, 01, and 11) for optical signal processing by controlling the laser power. As shown in Figure 5c, these four optical states correspond to no emission (00), the emission at 495 nm (10), the emission at 520 nm (01), and the emissions at 495 and 520 nm (11) simultaneously.

3. Conclusions

In summary, we proposed and demonstrated hybrid nanocavities composed of $CsPbBr_3$ nanoparticles and a thin Au film, which exhibit optically-controlled quantum size effect. The polycrystalline $CsPbBr_3$ nanoparticles used to create the hybrid nanocavities were synthesized by using chemical vapor deposition at a low temperature. The hybrid nanocavities exhibit dual-wavelength emission under the excitation of femtosecond laser pulses with a low repetition rate and their relative intensities can be manipulated by simply adjusting the excitation laser power. A phase transition from polycrystalline to monocrystalline can be induced by irradiating the nanoparticle with femtosecond laser pulses of a high repetition rate or a large power, leading to the conventional emission at 515 nm. Such a phase transition was confirmed by TEM observation and lifetime characterization. Four optical states can be achieved in the output of the hybrid nanocavity by deliberately controlling the laser power. Our findings indicate the potential applications of such hybrid nanocavities in optical display, optical sensing, and signal processing, and nanoscale light source.

4. Experimental Section

Synthesis and Characterization of $CsPbBr_3$ Nanoparticles: $CsPbBr_3$ nanoparticles were synthesized by using chemical vapor deposition.[15,53] The CsBr and $PbBr_2$ powders with molar ratio of 1:1 and total weight of ≈0.15 g were used as the vapor sources. They were mixed and placed at the center of a horizontal tube furnace. Two types of substrates (SiO_2 and Au/SiO_2) were placed away from the center in the downstream. The tube was firstly pumped to a pressure of 0.5 mTorr and then purified by using argon gas several times. After that, the temperature of the furnace was increased to 870 K within ≈20 min. After ≈40-min reaction, the tube furnace was cooled down to room temperature naturally.

The morphologies, structures, and composition of $CsPbBr_3$ nanoparticles were examined by SEM (Gemini 500, Zeiss) and TEM (JEM-2100HR). For TEM observations, $CsPbBr_3$ nanoparticles synthesized on a carbon-coated copper (Cu) grid were used. The Raman spectra of $CsPbBr_3$ nanoparticles were measured by using a 633-nm continuous-wave laser.

Optical Characterization: The femtosecond laser light (Mira 900S, Coherent) with a repetition rate of 76 or 3.8 MHz (obtained by using a pulse picker) and a duration of 130 fs was employed to excite $CsPbBr_3$

nanoparticles. A pulse picker (Coherent) was used to change the repetition rate of femtosecond laser pulses from 76 MHz to 3.8 or 2.9 MHz. It was focused on $CsPbBr_3$ nanoparticles by using the 100× objective lens of an inverted microscope (Axio Observer A1, Zeiss). For optical characterization, scattering light and PL were collected by using the same objective lens and directed to a spectrometer (SR-500i-B1, Andor) for analysis or to a coupled-charge device (DU970N, Andor) for imaging. The luminescence lifetimes of $CsPbBr_3$ nanoparticles were measured with a time-correlated single-photon system (lifespec II, Edinburgh Instruments).

Numerical Simulation and Analytical Model: The scattering spectra of $CsPbBr_3$ nanoparticles placed on a thin Au film were calculated numerically by using the finite-difference time-domain (FDTD) method (FDTD solution, https://www.lumerical.com). The complex refractive index of monocrystalline $CsPbBr_3$ was used in the calculation. The smallest mesh size was chosen to be 1.0 nm in order to obtain converged simulation results and perfectly matched layer boundary condition was employed to terminate the finite simulation region. The temperature distributions inside the hybrid nanocavities were calculated numerically based on the finite element method (COMSOL Multiphysics v5.5, https://www.comsol.com). The complex refractive index and thermal conductivity of monocrystalline $CsPbBr_3$ were taken from literature.[21,54,55]

Supporting Information

Supporting Information is available from the Wiley Online Library or from the author.

Acknowledgements

S.L. and M.Y. contributed equally to this work. S.L. and S.T. acknowledge the financial support from the National Key Research and Development Program of China (No. 2016YFA0201002), the National Natural Science Foundation of China (Grant Nos. 11674110 and 11874020), the Science and Technology Program of Guangzhou (No. 2019050001), and the Natural Science Foundation of Guangdong Province (Grant No. 2016A030308010). S.L. acknowledges the financial support from the Innovation Project of Graduate School of South China Normal University (No. 2019LKXM017).

Conflict of Interest

The authors declare no conflict of interest.

Keywords

gold film, nanocrystal, perovskite, phase transition, quantum dot

Received: November 3, 2020
Revised: November 26, 2020
Published online:

[1] Q. A. Akkerman, G. Rainò, M. V. Kovalenko, L. Manna, *Nat. Mater.* **2018**, *17*, 394.
[2] M. Yuan, L. N. Quan, R. Comin, G. Walters, R. Sabatini, O. Voznyy, S. Hoogland, Y. Zhao, E. M. Beauregard, P. Kanjanaboos, *Nat. Nanotechnol.* **2016**, *11*, 872.
[3] L. Protesescu, S. Yakunin, M. I. Bodnarchuk, F. Krieg, R. Caputo, C. H. Hendon, R. X. Yang, A. Walsh, M. V. Kovalenko, *Nano Lett.* **2015**, *15*, 3692.
[4] Q. Zhao, A. Hazarika, L. T. Schelhas, J. Liu, E. A. Gaulding, G. Li, M. Zhang, M. F. Toney, P. C. Sercel, J. M. Luther, *ACS Energy Lett.* **2019**, *5*, 238.
[5] K. Shen, H. Xu, X. Li, J. Guo, S. Sathasivam, M. Wang, A. Ren, K. L. Choy, I. P. Parkin, Z. Guo, J. Wu, *Adv. Mater.* **2020**, *32*, 2000004.
[6] S. Yakunin, B. M. Benin, Y. Shynkarenko, O. Nazarenko, M. I. Bodnarchuk, D. N. Dirin, C. Hofer, S. Cattaneo, M. V. Kovalenko, *Nat. Mater.* **2019**, *18*, 846.
[7] S. Shrestha, R. Fischer, G. J. Matt, P. Feldner, T. Michel, A. Osvet, I. Levchuk, B. Merle, S. Golkar, H. Chen, S. F. Tedde, O. Schmidt, R. Hock, M. Rührig, M. Göken, W. Heiss, G. Anton, C. J. Brabec, *Nat. Photonics* **2017**, *11*, 436.
[8] J.-P. Correa-Baena, M. Saliba, T. Buonassisi, M. Grätzel, A. Abate, W. Tress, A. Hagfeldt, *Science* **2017**, *358*, 739.
[9] M. Liu, M. B. Johnston, H. J. Snaith, *Nature* **2013**, *501*, 395.
[10] H. Lu, Y. Liu, P. Ahlawat, A. Mishra, W. R. Tress, F. T. Eickemeyer, Y. Yang, F. Fu, Z. Wang, C. E. Avalos, B. I. Carlsen, A. Agarwalla, X. Zhang, X. Li, Y. Zhan, S. M. Zakeeruddin, L. Emsley, U. Rothlisberger, L. Zheng, A. Hagfeldt, M. Grätzel, *Science* **2020**, 370.
[11] J. Xu, C. C. Boyd, J. Y. Zhengshan, A. F. Palmstrom, D. J. Witter, B. W. Larson, R. M. France, J. Werner, S. P. Harvey, E. J. Wolf, W. Weigand, S. Manzoor, M. F. A. M. V. Hest, J. J. Berry, J. M. Luther, Z. C. Holman, M. D. McGehee, *Science* **2020**, *367*, 1097.
[12] S. A. Veldhuis, P. P. Boix, N. Yantara, M. Li, T. C. Sum, N. Mathews, S. G. Mhaisalkar, *Adv. Mater.* **2016**, *28*, 6804.
[13] B. R. Sutherland, E. H. Sargent, *Nat. Photonics* **2016**, *10*, 295.
[14] Y. Liu, W. Yang, S. Xiao, N. Zhang, Y. Fan, G. Qu, Q. Song, *ACS Nano* **2019**, *13*, 10653.
[15] B. Tang, H. Dong, L. Sun, W. Zheng, Q. Wang, F. Sun, X. Jiang, A. Pan, L. Zhang, *ACS Nano* **2017**, *11*, 10681.
[16] H. Huang, A. S. Susha, S. V. Kershaw, T. F. Hung, A. L. Rogach, *Adv. Sci.* **2015**, *2*, 1500194.
[17] Q. Zhang, R. Su, X. Liu, J. Xing, T. C. Sum, Q. Xiong, *Adv. Funct. Mater.* **2016**, *26*, 6238.
[18] A. S. Berestennikov, P. M. Voroshilov, S. V. Makarov, Y. S. Kivshar, *Appl. Phys. Rev.* **2019**, *6*, 031307.
[19] S. Makarov, A. Furasova, E. Tiguntseva, A. Hemmetter, A. Berestennikov, A. Pushkarev, A. Zakhidov, Y. Kivshar, *Adv. Opt. Mater.* **2019**, *7*, 1800784.
[20] E. Y. Tiguntseva, D. G. Baranov, A. P. Pushkarev, B. Munkhbat, F. Komissarenko, M. Franckevicius, A. A. Zakhidov, T. Shegai, Y. S. Kivshar, S. V. Makarov, *Nano Lett.* **2018**, *18*, 5522.
[21] G. Murtaza, I. Ahmad, *Phys. B* **2011**, *406*, 3222.
[22] F. Deng, H. Liu, S. Lan, *Nanoscale Res. Lett.* **2018**, *13*, 395.
[23] J. Xiang, J. Chen, S. Jiang, M. Panmai, P. Li, Y. Xu, Q. Dai, S. Tie, S. Lan, *Laser Photonics Rev.* **2019**, *13*, 1800214.
[24] J. Xiang, J. Chen, S. Lan, A. E. Miroshnichenko, *Adv. Opt. Mater.* **2020**, *8*, 2000489.
[25] C. Lumdee, B. Yun, P. G. Kik, *ACS Photonics* **2014**, *1*, 1224.
[26] Z.-L. Deng, J. Deng, X. Zhuang, S. Wang, T. Shi, G. P. Wang, Y. Wang, J. Xu, Y. Cao, X. Wang, X. Cheng, G. Li, X. Li, *Light: Sci. Appl.* **2018**, *7*, 78.
[27] E. Xifre-Perez, L. Shi, U. Tuzer, R. Fenollosa, F. Ramiro-Manzano, R. Quidant, F. Meseguer, *ACS Nano* **2013**, *7*, 664.
[28] H. Li, Y. Xu, J. Xiang, X. Li, C. Zhang, S. Tie, S. Lan, *Nanoscale* **2016**, *8*, 18963.
[29] D. Parobek, Y. Dong, T. Qiao, D. H. Son, *Chem. Mater.* **2018**, *30*, 2939.
[30] A. Kojima, K. Teshima, Y. Shirai, T. Miyasaka, *J. Am. Chem. Soc.* **2009**, *131*, 6050.
[31] D. Han, M. Imran, M. Zhang, S. Chang, X.-G. Wu, X. Zhang, J. Tang, M. Wang, S. Ali, X. Li, *ACS Nano* **2018**, *12*, 8808.
[32] I. Levchuk, P. Herre, M. Brandl, A. Osvet, R. Hock, W. Peukert, P. Schweizer, E. Spiecker, M. Batentschuk, C. J. Brabec, *Chem. Commun.* **2017**, *53*, 244.
[33] W. Du, S. Zhang, Z. Wu, Q. Shang, Y. Mi, J. Chen, C. Qin, X. Qiu, Q. Zhang, X. Liu, *Nanoscale* **2019**, *11*, 3145.

[34] J. Xiang, S. Jiang, J. Chen, J. Li, Q. Dai, C. Zhang, Y. Xu, S. Tie, S. Lan, *Nano Lett.* **2017**, *17*, 4853.
[35] J. Zhao, S. Cao, Z. Li, N. Ma, *Chem. Mater.* **2018**, *30*, 6737.
[36] J. C. Beimborn, L. R. Walther, K. D. Wilson, J. M. Weber, *J. Phys. Chem. Lett.* **2020**, *11*, 1975.
[37] Z. Liang, S. Zhao, Z. Xu, B. Qiao, P. Song, D. Gao, X. Xu, *ACS Appl. Mater. Interfaces* **2016**, *8*, 28824.
[38] X. Huang, Q. Guo, D. Yang, X. Xiao, X. Liu, Z. Xia, F. Fan, J. Qiu, G. Dong, *Nat. Photonics* **2020**, *14*, 82.
[39] D. J. Slotcavage, H. I. Karunadasa, M. D. McGehee, *ACS Energy Lett.* **2016**, *1*, 1199.
[40] W. Mao, C. R. Hall, S. Bernardi, Y.-B. Cheng, A. Widmer-Cooper, T. A. Smith, U. Bach, *Nat. Mater.* **2020**, https://doi.org/10.1038/s41563-020-00826-y.
[41] W. Mao, C. R. Hall, A. S. Chesman, C. Forsyth, Y. B. Cheng, N. W. Duffy, T. A. Smith, U. Bach, *Angew. Chem., Int. Ed.* **2019**, *58*, 2893.
[42] Y. Zheng, H. Liu, J. Li, J. Xiang, M. Panmai, Q. Dai, Y. Xu, S. Tie, S. Lan, *Adv. Mater.* **2019**, *31*, 1901371.
[43] Z. Xue, H. Gao, W. Liu, X. Li, *ACS Appl. Electron. Mater.* **2019**, *1*, 2244.
[44] Z. Qin, S. Dai, V. G. Hadjiev, C. Wang, L. Xie, Y. Ni, C. Wu, G. Yang, S. Chen, L. Deng, Q. Yu, G. Feng, Z. M. Wang, J. Bao, *Chem. Mater.* **2019**, *31*, 9098.
[45] J.-H. Cha, J. H. Han, W. Yin, C. Park, Y. Park, T. K. Ahn, J. H. Cho, D.-Y. Jung, *J. Phys. Chem. Lett.* **2017**, *8*, 565.
[46] B. J. Bohn, Y. Tong, M. Gramlich, M. L. Lai, M. Döblinger, K. Wang, R. L. Hoye, P. Müller-Buschbaum, S. D. Stranks, A. S. Urban, L. Polavarapu, J. Feldmann, *Nano Lett.* **2018**, *18*, 5231.
[47] H. C. Wang, Z. Bao, H. Y. Tsai, A. C. Tang, R. S. Liu, *Small* **2018**, *14*, 1702433.
[48] S. N. Raja, Y. Bekenstein, M. A. Koc, S. Fischer, D. Zhang, L. Lin, R. O. Ritchie, P. Yang, A. P. Alivisatos, *ACS Appl. Mater. Interfaces* **2016**, *8*, 35523.
[49] L. Chen, G.-C. Li, G.-Y. Liu, Q.-F. Dai, S. Lan, S.-L. Tie, H.-D. Deng, *J. Phys. Chem. C* **2013**, *117*, 20146.
[50] S. Viarbitskaya, A. Teulle, R. Marty, J. Sharma, C. Girard, A. Arbouet, E. Dujardin, *Nat. Mater.* **2013**, *12*, 426.
[51] A. Krishna, S. Gottis, M. K. Nazeeruddin, F. Sauvage, *Adv. Funct. Mater.* **2019**, *29*, 1806482.
[52] Y.-S. Park, S. Guo, N. S. Makarov, V. I. Klimov, *ACS Nano* **2015**, *9*, 10386.
[53] S. Lan, W. Li, S. Wang, J. Li, J. Wang, H. Wang, H. Luo, D. Li, *Adv. Opt. Mater.* **2019**, *7*, 1801336.
[54] W. Lee, H. Li, A. B. Wong, D. Zhang, M. Lai, Y. Yu, Q. Kong, E. Lin, J. J. Urban, J. C. Grossman, P. Yang, *Proc. Natl. Acad. Sci. U. S. A.* **2017**, *114*, 8693.
[55] G. A. Elbaz, W.-L. Ong, E. A. Doud, P. Kim, D. W. Paley, X. Roy, J. A. Malen, *Nano Lett.* **2017**, *17*, 5734.